Comparative Studies of Nontoxic and Toxic Amyloids Interacting with Membrane Models at the Air−Water Interface

ARTICLE *in* LANGMUIR · MARCH 2011

Impact Factor: 4.46 · DOI: 10.1021/la103788r · Source: PubMed

Langmuir

ARTICLE

pubs.acs.org/Langmuir

Comparative Studies of Nontoxic and Toxic Amyloids Interacting with Membrane Models at the Air−Water Interface

Ha Phuong Ta,[†,‡] Karine Berthelot,[§] Bénédicte Coulary-Salin,[§] Bernard Desbat,[†] Julie Géan,[†] Laurent Servant,[‡] Christophe Cullin,[§] and Sophie Lecomte*[,†]

[†]Chimie et Biologie des Membranes et Nano-objets, Université de Bordeaux-CNRS, 2 rue Robert Escarpit, 33607 Pessac, France

[‡]Institut des Sciences Moléculaires, Université de Bordeaux-CNRS, 351 cours de la libération, 33405 Talence Cedex, France.

[§]Institut de Biochimie et Génétique Cellulaires, CNRS-Université Bordeaux 2 "Victor Segalen", 1 rue Camille Saint Saëns, 33077 Bordeaux Cedex, France

Supporting Information

ABSTRACT: Many in vitro studies have pointed out the interaction between amyloids and membranes, and their potential involvement in amyloid toxicity. In a previous study, we generated a yeast toxic mutant (M8) of the harmless model amyloid protein HET-s$_{(218-289)}$. In this study, we compared the self-assembling process of the nontoxic wild-type (WT) and toxic (M8) protein at the air−water interface and in interaction with various phospholipid monolayers (DOPE, DOPC, DOPI, DOPS and DOPG). We first demonstrate using ellipsometry measurements and polarization-modulated infrared reflection absorption spectroscopy (PMIRRAS) that the air−water interface promotes and modifies the assembly of WT since an amyloid-like film was instantaneously formed at the interface with an antiparallel β-sheet structuration instead of the parallel β-sheet commonly observed for amyloid fibers generated in solution. The toxic mutant (M8) behaves in a similar manner at the air−water interface or in bulk, with a fast self-assembling and an antiparallel β-sheet organization. The transmission electron microscopy (TEM) images established the fibrillous morphology of the protein films formed at the air−water interface. Second, we demonstrate for the first time that the main driving force between this particular fungus amyloid and membrane interaction is based on electrostatic interactions with negatively charged phospholipids (DOPG, DOPI, DOPS). Interestingly, the toxic mutant (M8) clearly induces perturbations of the negatively charged phospholipid monolayers, leading to a massive surface aggregation, whereas the nontoxic (WT) exhibits a slight effect on the membrane models. This study allows concluding that the toxicity of the M8 mutant could be due to its high propensity to interact with membranes.

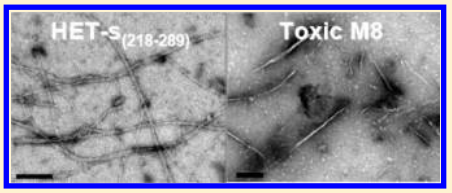

INTRODUCTION

More than 40 human pathologies are associated with amyloid proteins, and many are neurodegenerative disorders such as Alzheimer disease (amyloid-β, Aβ), Parkinson disease (α-synuclein) or Prion disease (PrP) (for review, see ref 1). Amyloids share common properties: association in fibrils, fibers, or aggregates with a cross-β sheet backbone and a classical 4.7 Å X-ray diffraction pattern. They also exhibit resistance to proteinases, and staining by various dyes as Thioflavine T or Congo red with which birefringence is observed. While numerous studies focused on pathological aspects, the origin of the amyloid toxicity remains unclear. Some authors have shed light on toxic intermediates of the fibrillization process, demonstrating that monomers,[2] oligomers,[3,4] and annular or short/quiescent fibrils[5−7] could be the toxic species. Others incriminate the deleterious formation of pores and channels into biological membranes.[8,9]

In the past decade, increasing evidence has shown that biological membranes are involved in amyloidogenesis (for review, see refs 10 and 11). Amyloids displayed toward lipids or membranes exhibit diverse properties: binding,[12] insertion,[13−15] disruption, and damages.[16−18] In addition, lipids may catalyze the aggregation process,[19,20] but it has also been shown with Aβ that natural lipids could resolubilize mature amyloid fibers into toxic protofibrils.[21] Lipid composition of the membrane may therefore impact the interaction of various amyloids with membranes in vivo.[16,18]

Amyloid bulk kinetics and structures may be significantly different from their interfacial characteristics,[22−24] which are more physiologically relevant. Langmuir monolayers therefore represent a convenient model system to mimic biological membranes and study amyloid interactions (for review, see ref 25), and infrared spectroscopy allows the characterization of secondary structures and their organizations at interfaces. Few Langmuir studies have been performed with amyloids, but many reports suggest that hydrophobic or negatively charged surfaces may promote nucleation or fibrillogenesis by favoring local concentration of proteins.[26−28] Studies at the air−water interface by compression isotherms demonstrated that hIAPP (Islet amyloid polypeptide involved in type 2 diabetes)[29] and various Aβ peptides were able to form highly stable monolayers.[18,30−33] These

Received: September 22, 2010
Revised: February 9, 2011
Published: March 15, 2011

amyloids were able to adhere and also insert into various negatively charged lipid monolayers, adopting a flat β-sheet conformation usually parallel to the surface.[29,31,34]

Our model amyloid is the prion-forming domain (PFD) of HET-s, a 289 amino protein of the filamentous fungus *Podospora anserina*. This protein is involved in a cell-death phenomenon termed heterocaryon incompatibility, which is able to control the cell fusion process. The prion domain HET-s$_{(218-289)}$ also assembles into an amyloid, which is nontoxic when expressed in the yeast *Saccharomyces cerevisiae*.[35] In a previous work, we generated a yeast toxic mutant called M8,[35] which differs from the wild-type (WT) by 10 mutations (see Supporting Information Figure 1S). In vivo, this mutant forms small dotted aggregates that differ from the annular WT large aggregates.[35] We previously biochemically and biophysically characterized the structural particularities of the M8 mutant fibers and their differences compared to the WT amyloid.[36] In vitro, WT amyloids exhibit some typical micrometer-long fibers, while M8 proteins assemble into 80 nm-long filaments; wide-angle X-ray scattering (WAXS) and attenuated total reflectance Fourier transform infrared (ATR-FTIR) allowed us to confirm that M8 fibrils were amyloids but with a totally different secondary structure based on an antiparallel organization of the β-sheets.[36] Moreover, M8 seems to clearly interfere in vivo with vesicular trafficking and membranes.[37] So far, no evidence of direct interactions between HET-s and membranes was investigated.

The complexity of biological membrane surfaces warrants the use of model membrane systems to investigate interactions between peripheral membrane proteins and phospholipids. Model systems constructed from monolayers rather than vesicles (bilayers) offer greater control over experimental variables such as surface density, surface pressure, subphase composition and molecular area. We use ellipsometry measurements and polarization-modulated infrared reflection absorption spectroscopy (PMIRRAS) to determine the morphological and structural properties of monolayers at the air−water interface. Ellipsometry images allow the visualization of the morphology of protein and lipid domains at the air−water interface, as well as changes in lipid monolayer organization after binding of the protein, with a spatial resolution in the micrometer order. The variations of measured ellipsometric angles allow the evaluation of the thickness of the layers present at the air−water interface. PMIRRAS gives access to the structure of the lipids, the protein secondary structure, and its orientation at the air−water interface.

In this paper, we first investigated the self-association of nontoxic amyloid (WT) versus toxic amyloid (M8) at the air−water interface. Second, in order to gain better insight into the toxicity and lipid binding specificities of the M8 mutant, we investigated the molecular interaction of toxic amyloid M8 compared to that of the nontoxic WT amyloid at the air−water interface with various kinds of lipids commonly found in yeast,[38,39] by ellipsometry and PMIRRAS. Herein we demonstrate the strong interaction of the toxic M8 amyloid with negatively charged lipids (DOPS, DOPI, and DOPG). In contrast, the interaction with the nontoxic amyloid is weaker, allowing us to propose that the toxicity of M8 could lie in its interaction with the membrane.

EXPERIMENTAL SECTION

PFD Purifications. The C-terminal histidine-tagged HET-s$_{(218-289)}$ constructs (WT and M8 ; Supporting Information Figure 1S) were purified as previously described.[36] For renaturation, the proteins were submitted to gel filtration on Hi-Trap Sephadex G-25 (GE Healthcare Europe GmbH, Orsay, France) at 4 °C, using 10 mM HCl pH 2.0 as the eluent. Subsequently, the pH was brought up to 7.4 by adding phosphate-buffered saline (PBS) 10× (1.37 M NaCl, 26.8 mM KCl, 101.4 mM Na_2HPO_4, 17.6 mM K_2HPO_4; MP Biomedicals Europe, Illkirch) at 1× final concentration. The physicochemical parameters of WT and M8 proteins are listed in Supporting Information Table 1S.

Chemicals. 1,2-Dioleoyl-*sn*-glycero-3-phospho-(1′-*rac*-glycerol) (sodium salt) (DOPG), 1,2-dioleoyl-*sn*-glycero-3-phospho-(1′-myo-inositol) (ammonium salt) (DOPI), 1,2-dioleoyl-*sn*-glycero-3-phospho-L-serine (sodium salt) (DOPS), 1,2-dioleoyl-*sn*-glycero-3-phosphocholine (DOPC), and 1,2-dioleoyl-*sn*-glycero-3-phosphoethanolamine (DOPE) were purchased from Avanti Polar Lipids, Inc. Organic solvents of HPLC grade were purchased from Aldrich (France). All other chemicals of the highest purity available were purchased from Sigma-Aldrich. Ultrapure water with a nominal resistivity of 18 mΩ·cm (Milli-Q, Millipore) was used for all the buffers.

Film Formation and Surface Pressure Measurements. Adsorption experiments were performed at 25 ± 1 °C on a circular Teflon trough (20.4 cm^2). The surface pressure (π) was measured with a plate of Whatman filter paper held by a Nima Wilhelmy balance. The trough was filled with 8 mL of PBS buffer (pH 7.4) or 10 mM HCl solution (pH 2.0). The surface tension of the water was measured at 72.8 mN/m. The interaction of WT or M8 with lipid films was performed in two steps. First, the lipids were spread at the air−water interface from chloroform/methanol (80%/20% v/v) solution at 0.2 mg/mL to reach the desired final surface pressure. Twenty minutes were required for solvent evaporation and pressure stabilization. Second, the proteins were injected into the subphase and stirred. The surface pressure was measured continuously until an equilibrium pressure was reached.

Ellipsometry Measurements. The thickness of the films formed was determined using a NFT IElli2000 ellipsometer (Göttingen, Germany) equipped with a doubled frequency Nd:YAG laser (532 nm, 50 mW), a polarizer, a compensating plate, an analyzer, and a CCD camera. It operates on the principle of classical null ellipsometry.[40] This parameter has been obtained from the ellipsometric angles (ψ and Δ) measured with an incidence angle of 54.58°, which give the null conditions. The morphology of films at the air−water interface was observed by the CCD camera. The spatial resolution was about 2 μm, and the size of images was 450 × 670 μm with a ×10 magnification lens used. The angles of the polarizer, compensator, and analyzer that obtained the null condition allow one to obtain the (Δ, Ψ) angles, which are related to the optical properties of the sample. For ultrathin films, Δ is proportional to the film thickness. Application of the measured data with computerized optical modeling included in the ellipsometric software leads to a deduction of film thickness for a given refractive index. The value of the film thickness mainly depends on the refractive index used. Since it is difficult to determine an accurate experimental refractive index value, we therefore decided to use the same average value of the refractive index 1.45 for both lipid layers and proteins to reduce the number of parameters introduced in our model.[41,42] We will discuss the results mainly by comparing the thickness of the various studied systems. The pictures presented in the various figures were corrected from the tilt angle observation.

Congo Red Binding and Birefringence. The protein (WT or M8) layers and the layers of lipid/WT or lipid/M8 presented at the air−water interface (0.75 μM, 25 °C after 3 h) were transferred by direct adsorption onto microscope glass coverslips (22 × 22 mm; Knittel Glaser, Germany). The glass coverslips were beforehand cleaned with CH_2Cl_2 to increase hydrophobicity and favor the adsorption of the films. Coverslips were then gently put in contact for 2 s with the interface (horizontal transfer) and let air-dried for 30 min. Adsorbed layers were

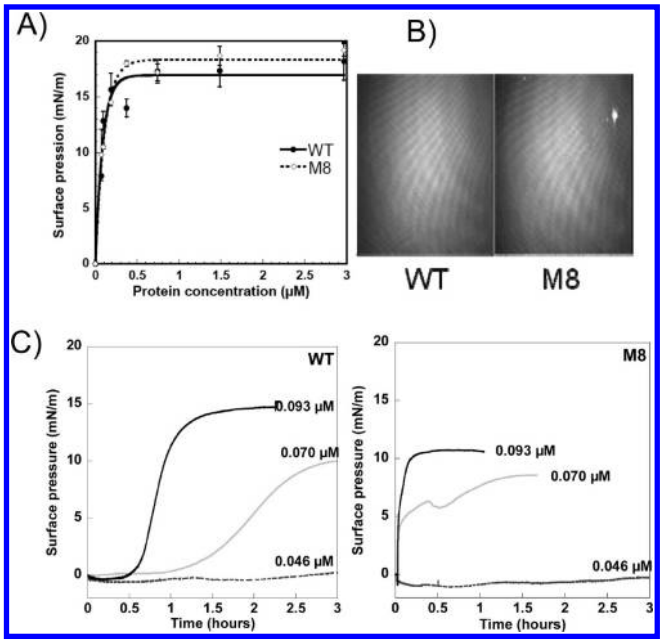

Figure 1. HET-s$(_{218-289})$ (WT) and its toxic Mutant 8 (M8) are surface active. (A) Surface pressure−protein concentration curves of WT and M8 at the air−water interface (PBS pH 7.4) and at equilibrium. (B) Ellipsometric images at equilibrium (0.75 μM in PBS after 180 min). The size of the images was 450 × 670 μm. (C) Surface pressure−time curves for different concentrations of proteins (WT and M8) at the air−water interface. Temperature was at 25 °C.

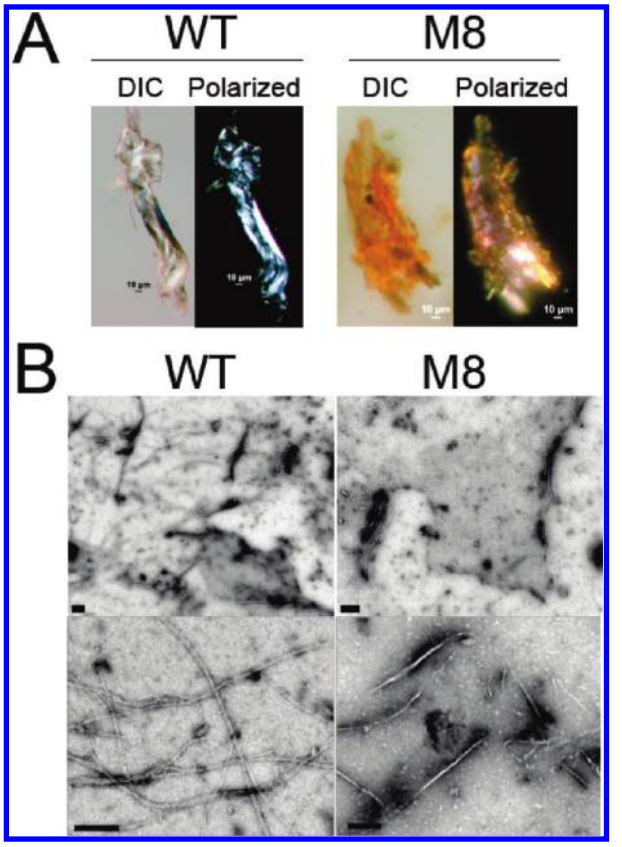

Figure 2. Fibrillous morphologies of WT and M8 films formed at the air−water interface. (A) Observation by light microscopy after staining with Congo red (left). Birefringence images (right) were observed under cross-polarized light. (B) TEM images of WT and M8 films. TEM scale bars represent 200 nm. For both microscopic observations, films were formed after protein injection of 0.75 μM in the PBS subphase at 25 °C. After 1 h 30 min (thickness of about 33 Å), the surface pressure was reached at 16 mN/m, and films were then transferred by direct adsorption onto glass coverslips or TEM grids.

then stained 2 s by incubation in a 20 μM Congo red solution in PBS buffer. Congo red binding and birefringence were observed with an ECLIPSE E600FN microscope (Nikon, Japan) with a PlanFluor 40× objective and a DXM1200 digital camera (Nikon) equipped with optimally aligned cross-polarizers.

Transmission Electron Microscopy (TEM). Protein films formed (0.75 μM, 25 °C after 1h30, thickness of about 33 Å) and visualized by ellipsometric microscopy were transferred for 2 s by adsorption onto Formvar-coated, carbon-stabilized copper grids (400 mesh) and allowed to dry for 15 min in air. Grids were then negatively stained 1 min with 10 μL of freshly prepared 2% uranyl acetate in water, dried with filter paper, and examined with a Hitachi H7650 transmission electron microscope (Hitachi, Krefeld, Germany) at an accelerating voltage of 120 kV. TEM was performed at the Pôle Imagerie Électronique of the Bordeaux Imaging Center.

PMIRRAS Measurements. PMIRRAS spectra were recorded on a Nicolet (Madison, WI) Nexus 870 spectrometer equipped with a HgCdTe (MCT) detector (SAT, Poitiers) and cooled at 77 K by nitrogen liquid at a resolution of 8 cm^{-1} by coadding 600 scans. Details of PMIRRAS experiments were described in a previous paper.[43] PMIRRAS spectra were normalized by the subphase spectrum. The room temperature was regulated at 25 ± 1 °C.

RESULTS

Amyloid-like Film Formations at the Air−Water Interface. Both nontoxic WT and toxic M8 proteins formed a homogeneous film at the air−water interface (Figure 1). Different protein concentrations from 0.046 μM to 2.969 μM were injected into the PBS subphase (pH 7.4). The surface pressure was measured continuously until equilibrium was reached. The surface pressure at the equilibrium increases with the concentration of WT or M8 in a similar manner to a maximum of about 18 mN/m, when the protein concentration is superior to 0.5 μM (Figure 1A). Ellipsometric images at equilibrium are also very similar (Figure 1B). Below 0.093 μM, the formation of WT monolayer at the air−water interface was preceded by a long lag phase (Figure 1C). For M8, the surface pressure increased just after injection even at 0.07 μM and no lag phase was observed (Figure 1C). Therefore, we could assume that M8 has a protein film formation faster than WT at the air−water interface, for low concentration. In solution, we previously demonstrated that the M8 toxic mutant assembly occurs through a totally different amyloidogenic pathway when compared to WT assembly.[44]

Results confirmed that under a specific threshold the protein adsorption kinetic depended strongly on protein quantity injected into the subphase.[30] Then, injection of 0.75 μM of WT or M8 leads to a maximum surface pressure, in equilibrium conditions. The variation of the ellipsometric angle ($\delta\Delta = 9.5°$ for both WT and M8) can be used to estimate the thickness of the film formed at the air−water interface. For a refractive index value of 1.45, we determined that both WT and M8 at equilibrium formed a homogeneous film of about 33 Å ± 3 Å.

The protein films formed at the surface (WT and M8) were transferred by adsorption and dried onto microscope coverslips and TEM grids. We know from our previous study that TEM

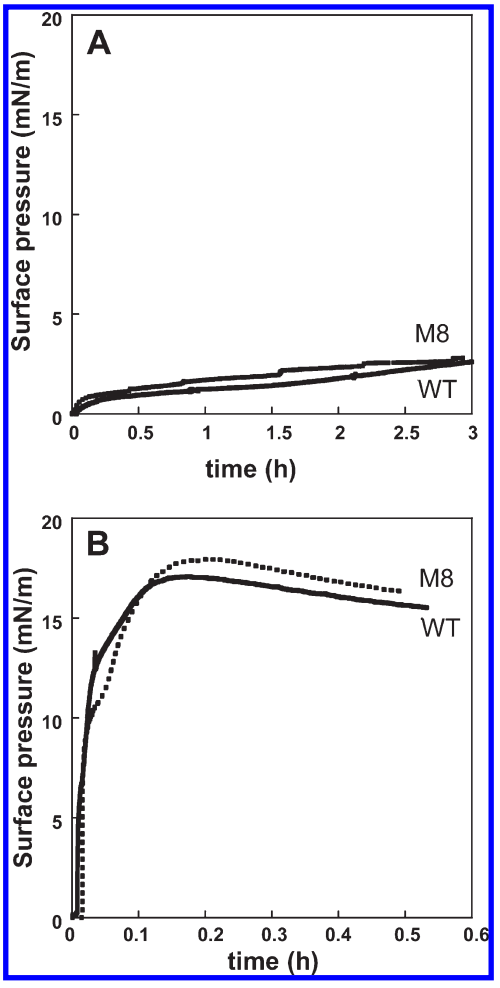

Figure 3. Pressure−time curves of WT and M8 adsorption process at air−water interface with a subphase at pH 2.0 (A) or at pH 7.4 (PBS) (B). Protein concentration was at 0.75 μM in PBS and temperature at 25 °C. NB: Different time scales, < 0.6 h for (B).

grids do not induce the polymerization of our amyloids in bulk,[44] and we assumed that the behavior was identical on glass coverslips. The samples adsorbed on microscope coverslips were then stained with Congo red dye. Observed under a microscope, the aggregates formed were quite "tissue-like", stained in red, and birefringent, which are classical amyloid characteristics (Figure 2A). We further analyzed these protein films by TEM after negative staining. A very dense fibrillar morphology was observed for the WT film (Figure 2B, top image), and the presence of numerous long fibers was detected. Indeed, our observations were very reminiscent of the amyloid fibers observed in bulk solution.[36] On the contrary, very few long fibers could be observed in the M8 film, but globally M8 forms much shorter fibers and fibrils than WT, and a large amount of small aggregates or intermediates are observed in the M8 film (white spots in Figure 2B; bottom large magnification). Nanofibers of about 80 nm and round oligomers were also a characteristic of M8 amyloidogenesis in bulk solution.[44] We previously established that the morphology of WT and M8 amyloid fibers formed in solution were also very different,[36] and we confirm also in this study that WT and M8 films differ in their molecular assembly. TEM and Congo red staining observations confirm that both WT and M8 are indeed fibrillar.

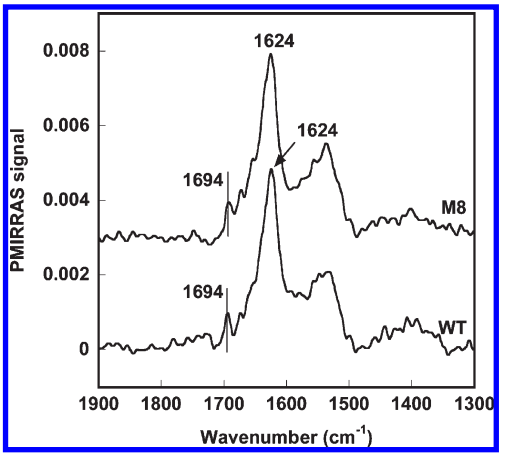

Figure 4. PMIRRAS spectra of WT and M8 aggregates at the air−water interface at pH 7.4. A cutoff of about 3×10^{-3} (PMIRRAS signal) is made between the two spectra to ensure a better observation. Protein concentration was at 0.75 μM in PBS and temperature at 25 °C. The pressure was around 16 mN/m.

Both WT and M8 proteins after purification at pH 2.0 are monomeric and unstructured.[44] A small increase of the surface pressure (2.5 mN/m) is observed if the subphase used is at pH 2.0 compared with a subphase at pH 7.4 (Figure 3). Then, the acidic interface cannot promote alone the formation of a compact peptide film at the interface (Figure 3A). Indeed the formation of WT and M8 films at the air−water interface is induced by the buffered subphase at pH 7.4, and at a concentration of 0.75 μM the kinetics of the assembling of both proteins does not present any lag phase (Figure 3B). With PBS as the subphase, the kinetic of film formation at the air−water interface is similar for the nontoxic and toxic-amyloid (Figure 3B). Ten minutes after the injection of the monomers, the maximum of surface pressure is reached and homogeneous films are formed at the air−water interface for both proteins. In addition, at the interface, we only observed a lag phase for WT at low concentrations (Figure 1B). Clearly bulk solution and interface self-assemblings are different, as WT polymerization exhibits a clear lag phase in bulk solution, even at a far higher concentration (50 μM).[44]

Figure 4 presents the PMIRRAS spectra of WT and M8 at the air−water interface, recorded 180 min after the injection of 0.75 μM of each protein in a monomeric form. In the amide I region 1600−1700 cm^{-1}, the spectra of WT or M8 aggregates showed an intense band at 1624 cm^{-1} and a faint shoulder at 1694 cm^{-1}, which is characteristic of an antiparallel β-sheet organization.[33,45] As known, an antiparallel β-sheet organization presents two components: one at low wavelength (between 1630 and 1620 cm^{-1}) and the second at higher wavelength (around 1680−1690 cm^{-1}) with an intensity ratio (I_{1690}/I_{1620}) from 1/8 to 1/10.[34,45] This explains why we observed a weak peak at 1690 cm^{-1} for both proteins. A parallel β-sheet signature would instead give a unique band around 1630 cm^{-1}, as previously observed by PMIRRAS.[46,47] Therefore, the profiles of both amide I and amide II bands are representative of antiparallel β-sheets mainly orientated parallel to the interface, as shown in previous works.[43,47] In conclusion, at the air−water interface, both proteins (WT and M8) have surface active properties, which organize as films with similar antiparallel β-sheet structures and amyloid-like properties (see above: stained by Congo red, birefringence, and fibrillous morphologies). This is clearly

dx.doi.org/10.1021/la103788r |*Langmuir* 2011, 27, 4797–4807

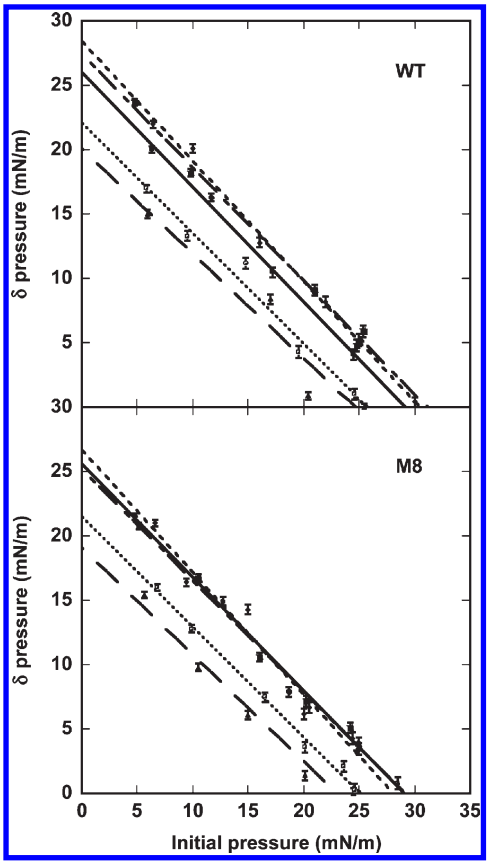

Figure 5. $\pi-\pi_i$ curves of the WT and the M8 interacting with monolayers of DOPI (●), DOPG (■), DOPS (♦), DOPC (▲), and DOPE (○). Protein concentration was 0.75 μM in PBS, and the temperature was 25 °C.

Table 1. MIP of the Proteins into Phospholipid Monolayers

	MIP (mN/m)	
	WT	M8
DOPC	24.7 ± 0.4	23.0 ± 0.4
DOPE	25.7 ± 0.5	25.2 ± 0.4
DOPI	29.2 ± 0.5	29.1 ± 0.5
DOPG	30.5 ± 0.5	29.2 ± 0.5
DOPS	30.5 ± 0.5	28.1 ± 0.5

different from the amyloid fibers formed in bulk solution, as WT is organized in parallel and M8 in antiparallel β-sheets (see Supporting Information Figure 2S).

Electrostatic Interaction Induces Insertion of M8 and WT in the Lipid Monolayers. To investigate the ability of WT and M8 to interact with a membrane, we formed monolayers of different phospholipids at the air−water interface and then injected unstructured proteins (pH 2.0) in the buffered subphase (PBS pH 7.4). Langmuir monolayers of negatively charged DOPS, DOPG, and DOPI and also zwitterionic DOPC and DOPE have been used. We carefully checked that no oxidation of the lipids occurs during the experiments following the surface pressure evolution. An oxidation of the lipids would induce a large decrease of the surface pressure, as described by Stottup et al.[48] Figure 5 illustrates the relationship between absolute

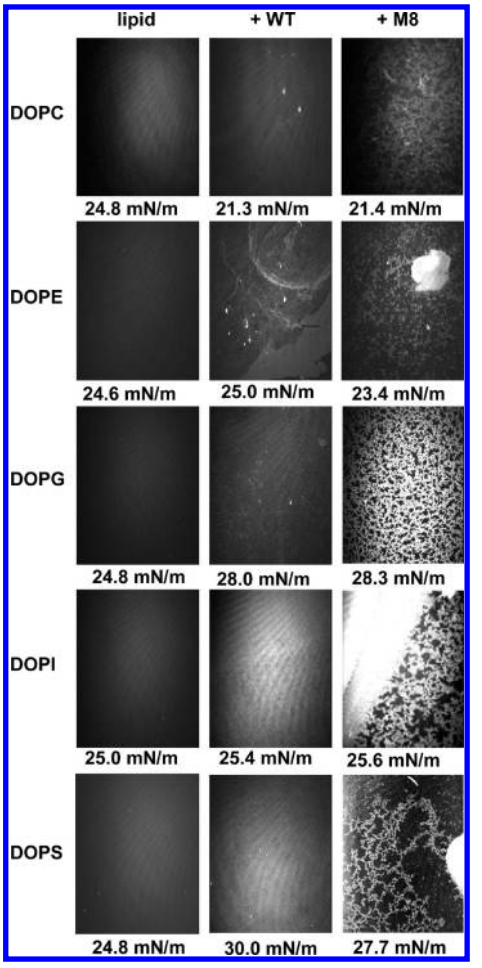

Figure 6. Ellipsometric images of DOPC, DOPE, DOPG, DOPI, and DOPS monolayers alone, and then after injection in the PBS subphase of 0.75 μM of WT and M8, respectively. Images were captured 180 min after protein injection. Surface pressure is indicated under each image. The size of the images was 450 × 670 μm.

increase in surface pressure ($\Delta\pi$) following injection of WT or M8 into the buffered subphase (pH 7.4) and the initial monolayer pressure (π_i). This graphical relationship generally reflects the relative insertion affinities to the Langmuir monolayer; higher values of the absolute increase in surface pressure indicate more pronounced insertion into the lipid monolayer. The sensitivity of both proteins to the five different monolayers of lipids are equal; indeed the slopes of the straight lines are very similar. The maximum insertion pressure (MIP), also called the critical insertion pressure (π_c), can be obtained by extrapolating the curve $\Delta\pi-\pi_i$ with the x axis. The obtained values are listed in Table 1. The MIP was observed between 24 and 25 mN/m for WT and M8 interacting with zwitterionic charged phospholipids, whereas an increase of the MIP (+4 or +5 mN/m) is observed with negatively charged lipids. Then, when the initial pressure was less than 25 mN/m, the insertion of both proteins resulted in pressure increases for all five tested phospholipids. With the initial pressure superior or equal to 25 mN/m, there was insertion only in the case of negatively charged phospholipids (DOPG, DOPS, and DOPI) with both proteins (Figure 5). Thus, both proteins have a stronger interaction with the anionic lipids than with the zwitterionic lipids. Considering the MIP of

dx.doi.org/10.1021/la103788r |*Langmuir* 2011, 27, 4797–4807

Table 2. Thickness of the Surface Layers and Ellipsometric Angles before and after Interaction with Proteins with PBS pH 7.4 as the Subphase[a]

	ellipsometric angle ($\delta\Delta$, Ψ) and layer thickness (Å)					
			lipid monolayer in interaction with			
	lipid monolayer		WT		M8	
	$\lvert\delta\Delta\rvert^\circ = \lvert\Delta - \Delta_0\rvert$ Ψ°	thickness (Å)	$\lvert\delta\Delta\rvert^\circ$ Ψ°	thickness (Å)	$\lvert\delta\Delta\rvert^\circ$ Ψ°	thickness (Å)
DOPC	4.7 ± 0.8	16 ± 2	6.4 ± 0.8	23 ± 3	10.4 ± 0.8	35 ± 4
	2.40 ± 0.12		2.39 ± 0.12		2.40 ± 0.12	
DOPE	4.9 ± 0.8	15 ± 2	14.1 ± 0.8	47 ± 4	13.7 ± 0.8	44 ± 4
	2.4 ± 0.12		2.37 ± 0.12		2.40 ± 0.12	
DOPG	4.5 ± 0.8	15 ± 2	6.0 ± 0.8	20 ± 2	21.0 ± 0.8	70 ± 6
	2.40 ± 0.12		2.40 ± 0.12		2.41 ± 0.12	
DOPI	5.6 ± 0.8	18 ± 1	13.6 ± 0.8	46 ± 5	32.5 ± 0.8	110 ± 11
	2.36 ± 0.12		2.37 ± 0.12		2.35 ± 0.12	
DOPS	4.8 ± 0.8	16 ± 1	10.6 ± 0.8	35 ± 3	29.2 ± 0.8	100 ± 9
	2.38 ± 0.12		2.38 ± 0.12		2.40 ± 0.12	

[a] The thickness was determined using a mean value of 1.45 for the refractive index. Results are presented as mean ± SD.

the M8 in comparison with the WT toward different phospholipids monolayers, no significant difference was demonstrated.

Toxic Amyloid (M8) Exhibits a Strong Interaction with Monolayer of Anionic Phospholipids. Although the variations of pressure are similar for M8 and WT in the presence of the studied phospholipid monolayers, ellipsometric images pointed out larger perturbations with the toxic mutant (M8) than with the WT (Figure 6). First, the ellipsometric images of the lipid monolayers alone at the initial surface pressure of around 25 mN/m show that homogeneous fluid films of lipids are formed at the air−water interface. The thickness of each phospholipid monolayer was calculated using a refractive index value of 1.45. Classical values were obtained for the phospholipid between 15 Å ± 2 Å and 16 Å ± 2 Å (see Table 2). Second, ellipsometric images of lipid monolayers in the presence of WT and M8 are presented 180 min after injection, and the surface pressure is indicated under each image (see Figure 6). As described before, an increase of the surface pressure was observed only with negatively charged phospholipids with both proteins. The films in the presence of WT always seem more homogeneous than those in the presence of M8. Stronger modifications with M8 were observed on the ellipsometric images revealing the presence of large aggregates when M8 interacts with monolayers of phospholipid, compared with WT. The brighter the aggregates are, the thicker the domains are. The thickness of the film in each case was determined from the ellipsometric angle variations and using a mean value for the refractive index (1.45) (Table 2). The difference in morphologies observed in Figure 6 images clearly revealed that the perturbation of the layers depends on specific interactions between proteins and lipids rather than on the insertion of protein into lipid layers. In the M8−lipids interaction, the appearance of aggregated domains at the air−water interface is common whatever the lipid, but the thickness of the layer increases for anionic lipids. The thicknesses (70 to 110 Å ± 10 Å) are multiplied by a factor of 5, comparing with pure DOPG, DOPI, or DOPS (15 to 16 Å ± 2 Å) . With zwitterionic lipids (DOPC, DOPE), despite very little or no insertion of M8 into the lipid layers, theses layers were considerably destabilized by the adsorption of proteins, as revealed by the observed aggregates (see Figure 6: M8+DOPC and M8+DOPE). In the WT−lipids interaction, although the surfaces were not homogeneous and they showed increased thickness at the surface (maximum ×3), the effects were obviously weaker. These results clearly demonstrated that the toxic M8 protein has significant effects toward phospholipid monolayers and more precisely with anionic phospholipids. We may suppose that the larger thickness observed for M8 indeed reflects a larger amount of M8 proteins (concentration effect) interacting with anionic lipids at the air−water interface.

WT and M8 Aggregates with Lipids Have Amyloid-like Properties. The macroscopic information on the protein (WT or M8)−lipid assembly at the air−water interface obtained by ellipsometry was then compared with PMIRRAS spectra, which provide information about the molecular structure. The PMIRRAS spectra of pure lipid monolayer in the 1800−1300 cm^{-1} range exhibit only one band at around 1730 cm^{-1}, assigned to the C═O elongation vibrational mode of the phospholipids. The broad negative peak at 1660 cm^{-1} is obviously associated with the $\delta(OH_2)$ deformation vibrational mode of the liquid water.[43] More precisely, this is due to the contrast of refraction index between lipid and water.[49] This phenomenon is observed in PMIRRAS spectra of compounds showing no absorption in the 1600−1700 cm^{-1} range, as for phospholipids.[43,47,50] In the case of peptides or proteins, it is more complex because the amide I has a strong absorption almost at the same frequency as that of the absorption of water. So the contrast between the refraction index of water and the refraction index of the protein layer is weak, and the experimental and simulation data show that the strong negative peak can almost completely disappear.[43,47,50] Depending on the orientation of the protein, this optical effect can appear or disappear.[43,47,50] When the β-sheet or α-helix are flat on the surface, the negative peak at 1660 cm^{-1} disappears, and when the β-sheet or α-helix are perpendicular (C═O group perpendicular to the surface) the negative peak appears. Such effect can be observed on the spectra of the pure proteins at the surface (Figure 4), where the relative intensities of the bands

dx.doi.org/10.1021/la103788r |*Langmuir* 2011, 27, 4797–4807

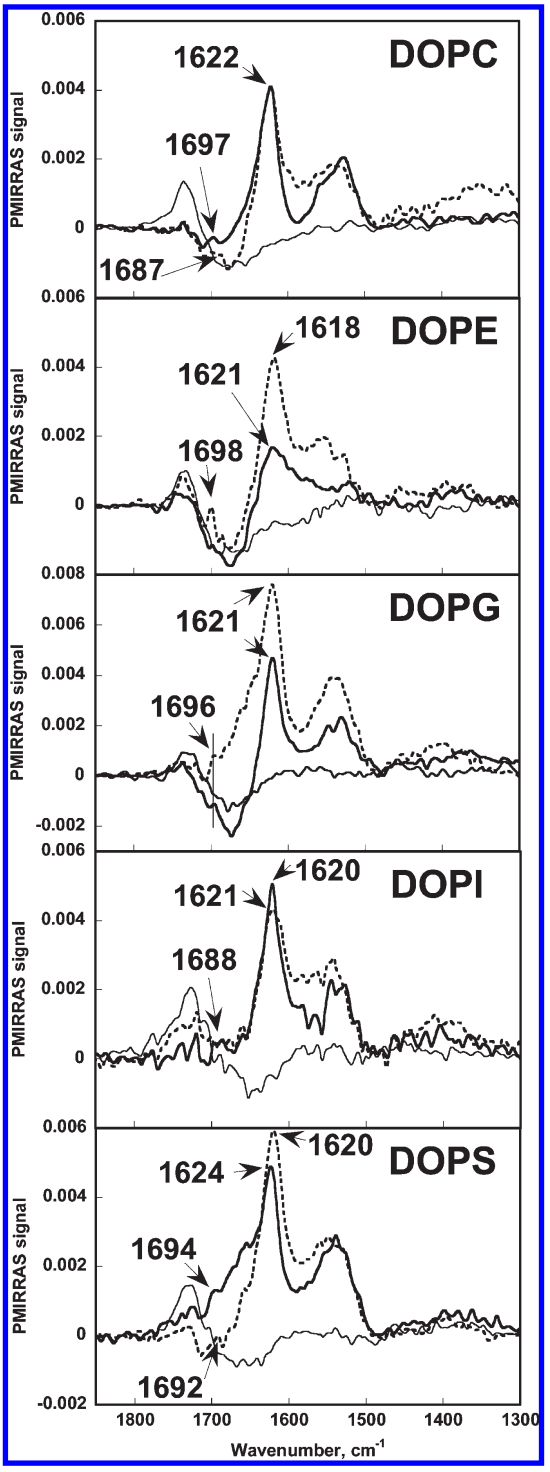

Figure 7. PMIRRAS spectra of the surface layer in protein−DOPC, DOPE, DOPG, DOPI, and DOPS interactions. Interactions are presented as lipid only (thin line), lipid−WT (bold line), and lipid−M8 (dotted line). The initial pressure of lipid monolayers was 25 mN/m.

indicate that the β-sheet is mainly in the plane. After adding protein, the PMIRRAS spectra displayed a large amide I band between 1600 and 1700 cm^{-1} and an amide II band at around 1535 cm^{-1} (Figure 7). For anionic phospholipids, the injection of WT or M8 in the subphase induces an increase of the surface pressure, and simultaneously the amide I and amide II bands are

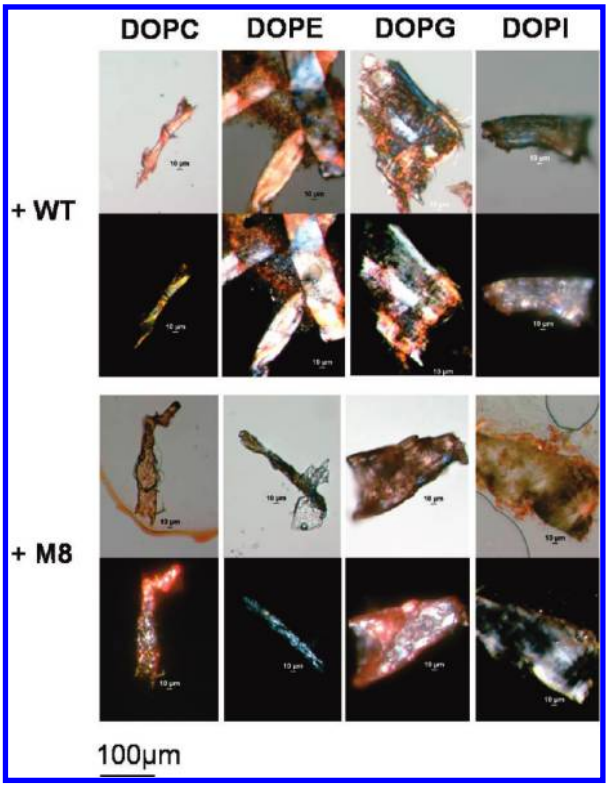

Figure 8. Congo red staining images of films formed at the air−water interface in bright field (top) and birefringence in cross-polarized light (bottom) of WT and M8 in interaction with DOPC, DOPE, DOPG, and DOPI. Films were formed at 0.75 μM in PBS, at 25 °C after 3 h. Pressures are reported in Figure 6.

observed. In the case of a zwitterionic lipid (DOPC, DOPE) the detection of the amide I and II bands appears with a delay (more than 60 min) (data not shown). After 3 h, at the equilibrium, for both proteins and all phospholipids studied, the profiles of the PMIRRAS spectra are similar with a maximum of amide I at 1622 cm^{-1} and small band at 1690 cm^{-1}, characteristic of an antiparallel β-sheet structure.[45,47] The thickness that can be probed by PMIRRAS at the air−water interface is around 200 nm, which is more than the phospholipid monolayer alone. Then, the observation of PMIRRAS spectra Figure 7 reveals that WT and M8 are in the proximity of the zwiterrionic phospholipid monolayer, whereas they did not induce an increase of the surface pressure. There were no observable significant differences in the secondary structure of the WT and the M8 in the interaction with phospholipid monolayers at the air−water interface.

The presence of intermolecular β-strands reveals the formation of amyloid interacting with the lipid monolayer. According to the PMIRRAS "surface selection rule" and considering the spectra features, both proteins are organized in antiparallel β-sheets in which the peptide chain was lightly tilted, i.e., the sheets were rather parallel to the interface plan.[47] Due to the higher thickness of the film with M8, we could expect an increase of the PMIRRAS spectra intensity for M8 interacting with lipid monolayers. However, we observed similar intensities for WT or M8 (see Figure 7). The slight variation observed on the amide I profiles of the various mixtures (amyloid/phospholipid monolayer) and the similar intensity observed can be explained by a variation of the angle of β-sheets with the plane of the interface that differ in the case of M8, compared to WT,[47] but also by the

dx.doi.org/10.1021/la103788r |*Langmuir* 2011, 27, 4797–4807

difference in the homogeneity of the films. So the PMIRRAS spectra were an average between the various domains presenting different densities of proteins interacting with lipids, at the air−water interface. The fact that the apparition of the proteins at the interface was concomitant with the decrease of both $\upsilon C{=}O$ intensity and in CH_2-CH_3 band intensity of hydrocarbon chain of lipids (see Figure S3) indicates that the lipid films were disturbed either by penetrating into the buffer or by changing orientation.

To confirm that the aggregates formed at the air−water interface in interaction with lipids have amyloid-like properties, we transferred the surface layers onto coverslips by direct contact as described above. The samples were then stained with Congo red dye and then were examined under microscope for staining and birefringence (Figure 8). All samples observed were stained very similarly to the protein films alone (Figure 2A), and were quite "tissue-like" or fibrous. Like at the air−water interface, in interaction with phospholipid monolayers, both types of transferred protein aggregates were stained in red, and displayed birefringence leading to the conclusion of the formation of WT and M8 aggregates in contact with lipids with amyloid-like properties.

DISCUSSION

In a previous work, we demonstrated the capacity for a harmless amyloid to be transformed into a toxic amyloid species (reducing considerably the growth of the yeast cell) by changing a few residues of the PFD of HET-s amyloid (HET-$s_{(218-289)}$).[35] However one major question is still asked: What makes an amyloid toxic? Several hypotheses can be proposed. First, many authors suggest that the amyloid toxicity is due to the "intermediates", from oligomers to protofilaments.[3−7] These intermediates are thought to form pores, which would destabilize the membranes but also change the cellular homeostasis.[8,9] In this study, we performed in vitro experiments using various monolayers of phospholipids at the air−water interface as model membranes, and analyzed their interactions with HET-s peptides (WT and M8 toxic mutant) by PMIRRAS and ellipsometry.

At first, we examined the behavior of WT and M8 only at the air−water interface. Both proteins demonstrate a surface activity; the maximum lateral pressure obtained was around 18 mN/m. Three criteria were taken into account to evaluate amyloid properties of proteins: (1) fibrillous morphology, (2) organization in β-sheet structure, and (3) amyloid staining with Congo red dye and birefringence. At pH 7.4, at the air−water interface, we demonstrated that the film aggregation of the two proteins adopted a similar antiparallel β-sheet conformation by PMIRRAS. Both WT and M8 aggregates were stained in red by Congo red, and showed birefringence when observed by cross-polarized light. TEM images reveal the fibrillous morphology of both films formed at the air−water interface. Our results point out that the air−water interface modifies both the kinetics of fibrillation and the secondary structure of the nontoxic amyloid (WT). Surprisingly, the process of amyloidogenesis of WT differs at the air−water interface compared to that in bulk solution. First, the air−water interface promotes the formation of an "amyloid-like film" with a new organization (antiparallel β-sheets), whereas in bulk solution the WT amyloid fibers were characterized by solid-state NMR (ssNMR) as a parallel β-sheet assembling.[51] The thickness of this amyloid film formed at the air−water interface (33 Å ± 3 Å) is also different from the size obtained for an individual WT fibril formed in solution (diameter about 5 nm; length up to a few micrometers[36]). A large polymorphism must be present in the subphase; however, at the air−water interface, we formed a stable, quite homogeneous film of proteins presenting fiber morphology with antiparallel β-sheet organization and amyloid-like properties. Yamazaki et al.[52] demonstrated by molecular dynamics experiments that the hydrophobic cooperativity plays an essential role in the formation of WT amyloid fibrils. A water channel was identified along the fibril axis playing an important role in the structural stability of fibrils.[52] The hydrophobic effect is the primary thermodynamic driving force in protein folding, while electrostatics provide mostly for specificity.[53] Then, we can conclude that the presence of the hydrophobic interface modifies the organization of the WT; the hydrophobic side chains can be exposed to the hydrophobic air, leading to an antiparallel β-sheet formation, as revealed by PMIRRAS. Second, the air−water interface increases the kinetics of the self-assembly of WT. PMIRRAS spectra recorded just following the injection of proteins (0.75 μM) immediately indicated an antiparallel β-sheet organization of WT. In solution, WT undergoes a molecular transition from random coils to a mainly parallel β-sheet organization. Indeed, at a far higher concentration (50 μM), in the same buffer, this structural transition followed by ATR-FTIR happens after a lag phase of about 40 min.[44] So, this demonstrated the acceleration role of the air−water interface in β-sheet formation. The differences of conformation and kinetics at the interface and in the bulk solution are evident for WT. Indeed, various proteins forming amyloid fibers in bulk solution are surface active and form stable Langmuir films differently structured at the air−water interface. This has been observed for amyloid-β films formed of either antiparallel β-sheets[31−34] or α-helices,[30] hIAPP and α-synuclein films also in α-helices,[29,54] or the LSFD peptide assembling in an antiparallel β-sheet monolayer.[31] For the toxic M8 mutant, the behavior at the air−water interface is quite comparable to the behavior in bulk solution. As in bulk, the process of film assembling is also fast, no lag phase was observed, and the same antiparallel signature was determined by ATR-FTIR.[36]

We aimed to understand the effect of each protein toward yeast plasma membrane components, in particular glycerophospholipids. The major phospholipids found in the membrane of *S. cerevisiae*, include PC, PE, PI, PS, and PG.[38,39,55] According to this fact and to the potential different interactions between the proteins and the polar head of phospholipids, we chose to analyze the lipid−amyloid interaction by using DOPI, DOPS, DOPG, DOPC, and DOPE in the Langmuir monolayer model. We report here the first study of the HET-s peptide interacting with membrane models. Our work demonstrates clearly the strong perturbation of anionic phospholipid monolayers by aggregation of the toxic amyloid (M8), compared to a nontoxic amyloid (WT). However, this difference cannot be explained by the primary sequences, as physicochemical properties are very similar for WT and M8 (see Supporting Information Table 1S). Large aggregates are observed on ellipsometric images of M8 interacting with DOPG, DOPI, and DOPS, which indicate that M8 probably not destabilize the monolayers by pore formation but by massive insertion in specific yeast membrane components. Very recently it has been shown that α-synuclein could exert its toxicity in yeast, causing trafficking defects by specific interaction with phosphatidic acid-rich membranes.[56] The adsorption of the nontoxic WT form is also observed; however, the effect is less drastic, with no segregation. The thickness of the layer present at

the air−lipid interface is 3 or 5 time bigger with M8 compared to WT. This in vitro behavior is in agreement with the in vivo experiments, which demonstrate that M8 interferes strongly with vesicular trafficking in yeast.[37] The data further illuminate that the charge of the lipid in our M8 specific interaction appears essential for initiating fibril formation. The electrostatic interaction is the driving force of protein−lipid interactions as demonstrated previously for various amyloids.[57] Such a behavior was also observed for IAPP in interaction with DOPC and DOPG layers[58] and hIAPP interacting with POPC and POPG monolayers using AFM.[29] Jha et al.[58] also demonstrated that with or without the air−water interface, anionic liposomes (DOPC/DOPG mixture) enhanced amyloid formation while DOPC did not. An antiparallel β-sheets conformation was detected for both amyloids (WT or M8) interacting with membranes, but the orientations of β-sheets under the phopholipid monolayer are different for WT and M8. In fact, the intensity ratio between amide I and amide II bands is sensitive to the orientation of β-sheet but as demonstrated by Banc et al.[47] it is rather the general shape of the amides domain (1700−1500 cm^{-1}), which is indicative of the orientation of this secondary structure. In our case, depending of the lipid used, the shapes of the domains for the WT and M8 types are systematically different. Moreover, the kinetics of film assembling of WT or M8 under phospholipid monolayers is different. Generally, the formation of amyloid-like films was observed earlier for M8 than for WT. So the effect of M8 is quite strong in comparison to the effect of Aβ(1−40) with a condensed phospholipid monolayer as demonstrated by Maltseva et al.[34] It does not only displace the lipids laterally as described for Aβ42 by Koppaka and Axelsen,[59] but a large aggregation is also observed. The layer damages are obviously evident through ellipsometric images; however, due to the limit of the instrument spatial resolution (1−2 μm), we could not deduce more clearly the molecular mechanism of membrane disruption.

In summary, we first demonstrate that the air−water interface, as model of hydrophobic−hydrophilic surface, promotes and modifies the self-assembling of HET-s$_{(218-289)}$. A different amyloid was instantaneously formed with a new secondary structure. An antiparallel β-sheet structuration was observed at the air−water interface instead of the parallel β-sheet commonly observed in solution. The toxic mutant (M8) behaves in a similar manner at the air−water interface or in bulk: fast self-assembling and antiparallel β-sheet organization. Second, we demonstrate for the first time that the main driving force for this fungus amyloid and membrane interaction is based on electrostatic interactions with negatively charged phospholipids. Interestingly, the toxic mutant (M8) clearly induces perturbations of negatively charged phospholipid monolayers, leading to a massive aggregation, whereas the nontoxic (WT) exhibits a slight effect on the membrane models. This study allows us to propose that the toxicity of the M8 mutant can be due to its high capability to interact with membranes, compared to the behavior of the WT, which is nontoxic in yeast.

■ ASSOCIATED CONTENT

Supporting Information. Physicochemical parameters of WT and M8 proteins, sequence of HET-s$_{(218-289)}$ (WT) and M8 toxic mutant, and ATR-FTIR spectra of WT and M8 amyloid fibers produced in bulk solution. This material is available free of charge via the Internet at http://pubs.acs.org.

■ AUTHOR INFORMATION

Corresponding Author

*E-mail: s.lecomte@cbmn.u-bordeaux.fr. Fax: (33) 5 40 00 22 00.

■ ACKNOWLEDGMENT

We are grateful to Dr. Reiko Oda for kindly allowing us access to her polarized microscope at IECB, Pessac. H.P.T. received a fellowship from the French Ministry of Research, and K.B. received a fellowship from the Conseil Régional d'Aquitaine. This work was supported by a grant from the Centre National de la Recherche Scientifique (Interface Chimie Biologie Physique: Soutien à la prise de risque).

■ ABBREVIATIONS USED:

PFD, prion-forming domain; CR, Congo red; PMIRRAS, polarization modulation infrared reflection absorption spectroscopy

■ REFERENCES

(1) Chiti, F.; Dobson, C. M. Protein misfolding, functional amyloid, and human disease. *Annu. Rev. Biochem.* **2006**, *75*, 333–366.

(2) Nagai, Y.; Inui, T.; Popiel, H. A.; Fujikake, N.; Hasegawa, K.; Urade, Y.; Goto, Y.; Naiki, H.; Toda, T. A toxic monomeric conformer of the polyglutamine protein. *Nat. Struct. Mol. Biol.* **2007**, *14*, 332–340.

(3) Kayed, R.; Head, E.; Thompson, J. L.; McIntire, T. M.; Milton, S. C.; Cotman, C. W.; Glabe, C. Common structure of soluble amyloid oligomers implies common mechanism of pathogenesis. *Science* **2003**, *300*, 486–489.

(4) Bucciantini, M.; Giannoni, E.; Chiti, F.; Baroni, F.; Formigli, L.; Zurdo, J.; Taddei, N.; Ramponi, G.; Dobson, C. M.; Stefani, M. Inherent toxicity of aggregates implies a common mechanism for protein misfolding diseases. *Nature* **2002**, *416*, 507–511.

(5) Xue, W. F.; Hellewell, A. L.; Gosal, W. S.; Homans, S. W.; Hewitt, E. W.; Radford, S. E. Fibril fragmentation enhances amyloid cytotoxicity. *J. Biol. Chem.* **2009**, *284*, 34272–34282.

(6) Petkova, A. T.; Leapman, R. D.; Guo, Z.; Yau, W. M.; Mattson, M. P.; Tycko, R. Self-propagating, molecular-level polymorphism in Alzheimer's β-amyloid fibrils. *Science* **2005**, *307*, 262–265.

(7) Kayed, R.; Pensalfini, A.; Margol, L.; Sokolov, Y.; Sarsoza, F.; Head, E.; Hall, J.; Glabe, C. Annular protofibrils are a structurally and functionally distinct type of amyloid oligomer. *J. Biol. Chem.* **2009**, *284*, 4230–4237.

(8) Quist, A.; Doudevski, I.; Lin, H.; Azimova, R.; Ng, D.; Frangione, B.; Kagan, B.; Ghiso, J.; Lal, R. Amyloid ion channels: A common structural link for protein-misfolding disease. *Proc. Natl. Acad. Sci. U.S.A.* **2005**, *102*, 10427–10432.

(9) Lashuel, H. A.; Hartley, D.; Petre, B. M.; Walz, T.; Lansbury, P. T. Neurodegenerative disease: Amyloid pores from pathogenic mutations. *Nature* **2002**, *418*, 291.

(10) Hebda, J.; Miranker, A. The interplay of catalysis and toxicity by amyloid intermediates on lipid bilayers: Insights from type II diabetes. *Annu. Rev. Biophys.* **2009**, *38*, 125–52.

(11) Aisenbrey, C.; Borowik, T.; Byström, R.; Bokvist, M.; Lindström, F.; Misiak, H.; Sani, M.-A.; Gröbner, G. How is protein aggregation in amyloidogenic diseases modulated by biological membranes?. *Eur. Biophys. J.* **2008**, *37*, 247–255.

(12) Hertel, C.; Terzi, E.; Hauser, N.; Jakob-Rotne, R.; Seelig, J.; Kemp, J. A. Inhibition of the electrostatic interaction between beta-amyloid peptide and membranes prevents β-amyloid-induced toxicity. *Proc. Natl. Acad. Sci. U.S.A.* **1997**, *94*, 9412–9416.

(13) Engel, M. F.; Yigittop, H.; Elgersma, R. C.; Rijkers, D. T.; Liskamp, R. M.; de Kruijff, B.; Höppener, J. W.; Killian, J. A. Islet amyloid polypeptide inserts into phospholipid monolayers as monomer. *J. Mol. Biol.* **2006**, *356*, 783–789.

(14) Baron, G. S. Conversion of raft associated prion protein to the protease-resistant requires insertion of PrP-res (PrPSc) into contiguous membranes. *EMBO J.* **2002**, *21*, 1031–1040.
(15) Mason, R. P.; Jacob, R. F.; Walter, M. F.; Mason, P. E.; Avdulov, N. A.; Chochina, S. V.; Igbavboa, U.; Wood, W. G. Distribution and fluidizing action of soluble and aggregated amyloid β-peptide in rat synaptic plasma membranes. *J. Biol. Chem.* **1999**, *274*, 18801–18807.
(16) Engel, M. F. M.; Khemtémourian, L.; Kleijer, C. C.; Meeldijk, H. J. D.; Jacobs, J.; Verkleij, A. J.; de Kruijff, B.; Killian, J. A.; Höppener, J. W. M. Membrane damage by human islet amyloid polypeptide through fibril growth at the membrane. *Proc. Natl. Acad. Sci. U.S.A.* **2008**, *105*, 6033–6038.
(17) Kayed, R.; Sokolov, Y.; Edmond, B.; McIntire, M.-T.; Milton, S. C.; Hall, J. E.; Glabe, C. G. Permeabilization of lipid bilayers is a common conformation-dependent activity of soluble amyloid oligomers in protein misfolding diseases. *J. Biol. Chem.* **2004**, *279*, 46363–46366.
(18) Ambroggio, E. E.; Kim, D. H.; Separovic, F.; Barrow, C. J.; Barnham, K. J.; Bagatolli, L. A.; Fidelio, G. D. Surface behavior and lipid interaction of Alzheimer β-amyloid peptide1−42: A membrane-disrupting peptide. *Biophys. J.* **2005**, *88*, 2706–2713.
(19) Choo-Smith, L. P.; Garzon-Rodriguez, W.; Glabe, C. G.; Surewicz, W. K. Acceleration of amyloid fibril formation by specific binding of Aβ-(1−40) peptide to ganglioside-containing membrane vesicles. *J. Biol. Chem.* **1997**, *272*, 22987–22990.
(20) Necula, M.; Chirita, C. N.; Kuret, J. Rapid anionic micelle-mediated α-synuclein fibrillization in vitro. *J. Biol. Chem.* **2003**, *278*, 46674–46680.
(21) Martins, I. C.; Kuperstein, I.; Wilkinson, H.; Maes, E.; Vanbraban, M.; Jonckheere, W.; Van Gelder, P.; Hartmann, D.; D'Hooge, R.; De Strooper, B.; Schymkowitz, J.; Rousseau, F. Lipids revert inert Aβ amyloid fibrils to neurotoxic protofibrils that affect learning in mice. *EMBO J.* **2008**, *27*, 224–233.
(22) Kakio, A.; Yano, Y.; Takai, D.; Kuroda, Y.; Matsumoto, O.; Kozutsumi, Y.; Matsuzaki, K. Interaction between amyloid Aβ-protein aggregates and membranes. *J. Pept. Sci.* **2004**, *10*, 612–621.
(23) Jean, L.; Lee, C. F.; Lee, C.; Shaw, M.; Vaux, D. J. Competing discrete interfacial effects are critical for amyloidogenesis. *FASEB J.* **2010**, *24*, 309–317.
(24) Zhu, M.; Souillac, P. O.; Ionescu-Zanetti, C.; Carter, S. A.; Fink, A. L. Surface-catalyzed amyloid fibril formation. *J. Biol. Chem.* **2002**, *277*, 50914–50922.
(25) Takur, G.; Micic, M.; Leblanc, R. M. Surface chemistry of Alzeimer's disease: A Langmuir monolayer approach. *Colloids Surf., B* **2009**, *74*, 436–456.
(26) Dorosz, J.; Volinsky, R.; Bazar, E.; Kolusheva, S.; Jelinek, R. Phospholipid-induced fibrillation of a prion amyloidogenic determinant at the air/water interface. *Langmuir* **2009**, *25*, 12501–12506.
(27) Nayak, A.; Dutta, A. K.; Belfort, G. Surface-enhanced nucleation of insulin amyloid fibrillation. *Biophys. Biochim. Res. Commun.* **2008**, *369*, 303–307.
(28) Linse, S.; Cabaleiro-Lago, C.; Xue, W.-F.; Lynch, I.; Lindman, S.; Thulin, E.; Radford, S. E.; Dawson, K. A. Nucleation of protein fibrillation by nanoparticles. *Proc. Natl. Acad. Sci. U.S.A.* **2007**, *104*, 8691–8696.
(29) Lopes, D. H. J.; Meister, A.; Gohlke, A.; Hauser, A.; Blume, A.; Winter, R. Mechanism of islet amyloid polypeptide fibrillation at lipid interfaces studied by infrared reflection absorption spectroscopy. *Biophys. J.* **2007**, *93*, 3132–3141.
(30) Jiang, D.; Dinh, K. L.; Ruthenburg, T. C.; Zhang, Y.; Su, L.; Land, D. P.; Zhou, F. A kinetic model for β-amyloid adsorption at the air/solution interface and its implication to the β-amyloid aggregation process. *J. Phys. Chem. B* **2009**, *113* (10), 3160–3168.
(31) Lepère, M.; Muenter, A. H.; Chevallard, C.; Gueboun, P.; Brezesinski, G. Comparative IR and X-ray studies of natural and model amyloid peptides at the air/water interface. *Colloids Surf., A* **2007**, *303*, 73–78.
(32) Maltseva, E.; Brezesinski, G. Adsorption of amyloid beta (1−40) peptide to phosphatidylethanolamine monolayers. *ChemPhysChem.* **2004**, *5*, 1185–1190.
(33) Schladitz, C.; Vieira, E. P.; Hermel, H.; Möhwald, H. Amyloid β-sheet formation at the air−water interface. *Biophys. J.* **1999**, *77*, 3305–3310.
(34) Maltseva, E.; Kerth, A.; Blume, A.; Möhwald, H.; Brezesinski, G. Adsorption of amyloid beta (1−40) peptide at phospholipid monolayers. *ChemBioChem.* **2005**, *6* (10), 1817–1824.
(35) Couthouis, J.; Rébora, K.; Immel, F.; Berthelot, K.; Castroviejo, M.; Cullin, C. Screening for toxic amyloid in yeast exemplifies the role of alternative pathway responsible for cytotoxicity. *PLoS One* **2009**, *4*, e4539.
(36) Berthelot, K.; Immel, F.; Géan, J.; Lecomte, S.; Oda, R.; Kauffmann, B.; Cullin, C. Driving amyloid toxicity in a yeast model by structural changes: A molecular approach. *FASEB J.* **2009**, *23*, 2254–2263.
(37) Couthouis, J.; Marchal, C.; D'Angelo, F.; Berthelot, K.; Cullin, C. The toxicity of an "artificial" amyloid is related to how it interacts with membranes. *Prion* **2010**, *4* (4), 283–291.
(38) Van der Rest, M. E.; Kamminga, A. H.; Nakano, A.; Anraku, Y.; Poolman, B.; Konings, W. N. The plasma membrane of saccharomyces cerevisiae: Structure, function, and biogenesis. *Microbiol. Rev.* **1995**, *59*, 304–322.
(39) Carman, G. C.; Henry, S. A. Phospholipid biosynthesis in the yeast *Saccharomyces cerevisiae* and interrelationship with other metabolic processes. *Prog. Lipid Res.* **1999**, *38*, 361–399.
(40) Azzam, R. M. A.; Bashara, N. M. *Ellipsometry and Polarized Light*; North-Holland Physics Publishing: New York, 1977.
(41) Ducharme, D.; Max, J. J.; Salesse, C.; Leblanc, R. M. Ellipsometric study of the physical state of phosphatidylcholines at the air−water interface. *J. Phys. Chem.* **1990**, *94*, 1925–1932.
(42) Saccani, J.; Castano, S.; Beaurain, F.; Laguerre, M.; Desbat, B. Stabilization of phospholipid multilayers at the air−water interface by compression beyond the collapse: A BAM, PM-IRRAS and molecular dynamics study. *Langmuir* **2004**, *20*, 9190–9197.
(43) Blaudez, D.; Turlet, J. M.; Dufourcq, J.; Bard, D.; Buffeteau, T.; Desbat, B. Investigation at air−water interface using polarization modulation IR spectroscopy. *J.Chem. Soc., Faraday Trans.* **1996**, *92*, 525–530.
(44) Berthelot, K.; Lecomte, S.; Géan, J.; Immel, F.; Cullin, C. A yeast toxic mutant of HET-s(218−289) prion displays alternative intermediates of amyloidogenesis. *Biophys. J.* **2010**, *99*, 1239–1246.
(45) Goormaghtigh, E.; Cabiaux, V.; Ruysschaert, J. M. Determination of soluble and membrane protein structure by Fourier transform infrared. In *Physicochemical Methods in the Study of Biomembranes*; Hilderson, H. J., Ralson, G. B., Eds.; Plenum Press: New York, 1994; Vol. 23, pp 405−450.
(46) Ronzon, F.; Desbat, B.; Chauvet, J. P.; Roux, B. Behavior of a GPI-anchored protein in phospholipid monolayers at the air−water interface. *Biochim. Biophys. Acta* **2002**, *1560*, 1–13.
(47) Banc, A.; Desbat, B.; Renard, D.; Popineau, Y.; Mangavel, C.; Navailles, L. Structure and orientation changes of ω- and γ-gliadins at the air−water interface: A PM-IRRAS spectroscopy and Brewster angle microscopy study. *Langmuir* **2007**, *23*, 13066–13075.
(48) Stottrup, B. L.; Stevens, D. S.; Keller, S. L. Miscibility of ternary mixtures of phospholipids and cholesterol in monolayers, and application to bilayer systems. *Biophys. J.* **2005**, *88*, 269–276.
(49) Bertie, J. E.; Lan, Z. D. Infrared intensities of liquids 20. The intensity of the OH band of liquid water revisited, and the best current values of the optical constants of $H_2O(1)$ at 25°C between 15,000 and 1 cm^{-1}. *Appl. Spectrosc.* **1996**, *43*, 1047–1057.
(50) Cornut, I.; Desbat, B.; Turlet, J. M.; Dufourcq, J. *In situ* study by polarization modulated Fourier transform infrared spectroscopy of the structure and orientation of lipids and amphipatic peptides at air−water interface. *Biophys. J.* **1996**, *70*, 305–312.
(51) Wasmer, C.; Lange, A.; Van Melckebeke, H.; Siemer, A. B.; Riek, B.; Meier, H. Amyloid fibrils of the HET-s(218−289) prion form a β soleinoid with a triangle hydrophobic core. *Science* **2008**, *319*, 523–1526.
(52) Yamazaki, T.; Blinov, N.; Wishart, D.; Kovalenko, A. Hydration effects on the HET-s prion and amyloid-β fibrillous aggregates, studied

with three-dimensional molecular theory of solvation. *Biophys. J.* **2008**, *95*, 4540–4548.

(53) Hills, R. D.; Brooks, C. L., III. Hydrophobic cooperativity as a mechanism for amyloid nucleation. *J. Mol. Biol.* **2007**, *368*, 894–901.

(54) Wang, C.; Shah, N.; Thakur, G.; Zhou, F.; Leblanc, R. M. α-Synuclein in α-helical conformation at air−water interface: Implication of conformation and orientation changes during its accumulation/aggregation. *Chem. Commun.* **2010**, *46*, 6702–6704.

(55) Zinser, E.; Sperka-Gottlieb, C. D. M.; Fasch, E.-V.; Kohlwein, S. D.; Paltauf, F.; Daum, G. Phospholipid synthesis and lipid composition of subcellular membranes in the unicellular eukaryote *Saccharomyces cerevisiae*. *J. Bacteriol.* **1991**, *173*, 2026–2034.

(56) Soper, J. H.; Kehm, V.; Burd, C. G.; Bankaitis, V. A.; Lee, V. M.-Y. Aggregation of α-synuclein in *S. cerevisiae* is associated with defects in endosomal trafficking and phospholipid biosynthesis. *J. Mol. Neurosci.* **2011**, *43*, 391–405.

(57) Relini, A.; Cavalleri, O.; Rolandia, R.; Gliozzi, A. The two-fold aspect of the interplay of amyloidogenic proteins with lipid membranes. *Chem. Phys. Lipids* **2009**, *158*, 1–9.

(58) Jha, S.; Sellin, D.; Seidel, R.; Winter, R. Amyloidogenic propensities and conformational properties of ProIAPP and IAPP in the presence of lipid bilayer membranes. *J. Mol. Biol.* **2009**, *389*, 907–920.

(59) Koppaka, V.; Axelsen, P. H. Accelerated accumulation of amyloid β proteins on oxidatively damaged lipid membranes. *Biochemistry* **2000**, *39*, 10011–10016.